

Combined effects of pulsatile flow and dynamic curvature on wall shear stress in a coronary artery bifurcation model

I.V. Pivkin¹, P.D. Richardson², D.H. Laidlaw³ and G.E. Karniadakis^{1*}

¹ Division of Applied Mathematics

² Division of Engineering

³ Department of Computer Science
Brown University

October 29, 2003

Abstract

A three-dimensional model with simplified geometry for the coronary artery is presented. In particular, both bifurcation and multi-planar curvature are included in the geometry of the computational domain. The model takes into account the repetitive variation of curvature and motion to which the vessel is subject during each cardiac cycle. It also accounts for the phase difference between arterial motion and flowrate that may be nonzero for patients with aortic regurgitation. An arbitrary Lagrangian Eulerian (ALE) formulation of the unsteady, incompressible, three dimensional Navier-Stokes equations is employed to solve for the flow field, while a velocity smoothing method is used for updating the computational mesh. Numerical simulations are performed using the spectral/*hp* element method. The results suggest that the combined effect of pulsatile inflow and dynamic geometry has significant influence on the flow dynamics and wall shear rate in a model of a coronary artery at bifurcation. Specifically, the main findings of this work relate to the time-variation of flowrate ratio between the two branches, and the change in shear rate distribution on the myocardial wall, especially for nonzero phase difference.

*Corresponding Author, gk@dam.brown.edu

1 Introduction

Histology studies have shown that atherosclerosis is likely to develop in preferred locations, including the inner walls of curvatures of carotid and coronary arteries [1, 2]. Some studies also have shown that intimal thickening that leads to atherosclerosis is often observed at bifurcations on the outer wall of side vessel, opposite to flow divider [2, 3]. It is widely believed that the complex flow field occurring in curvatures and bifurcations of large and medium arteries is related to the development and progression of the disease. Specifically, it has been shown that there is a positive correlation between atherosclerosis lesion locations and low and oscillating wall shear stresses [2, 4].

Numerical studies based on rigid, idealized [5, 6] as well as realistic [7, 8] model geometries were found to be useful in understanding the unique complex features associated with these flows. The majority of these investigations were focused on the geometry, pulsatile flow and non-Newtonian behavior of blood in non-moving vessels. The effect of distensible wall on the local flow field was analyzed in [9, 10]. Some authors have suggested that the flexibility and motion of coronary artery during each contraction and expansion of the heart is important in the study of the flow dynamics. Several investigations used models where the vessel was represented by a single flexible tube [11, 12, 13].

Comparatively less is known about the effects of vessel movement on the blood flow patterns in coronary arteries at *bifurcation*. However, it is known that as coronary artery passes across the surface of the heart, small branches come off and end in a rich network of arteries and capillaries [14]. In [11] a realistic arterial motion was simulated based on biplane cineangiograms in human right coronary arteries but without considering any branches. Weydahl & Moore were among the first to consider the model of coronary artery at bifurcation with time-varying geometry in [15]. They showed that the effects of curvature variation are important in determining temporal wall shear stress variations. However, they only considered steady inflow in their studies.

The objective of the present work is to analyse the *combined effect* of dynamic geometry and pulsatile inflow on the flow dynamics and wall shear rate in a model of a coronary artery at bifurcation. This will allow us to account for any phase lag between the two unsteady phenomena that may arise in cardiac disease. In the simulation, the main problem is how best to represent the curvature of the arterial segment for which computation is performed, and also the temporal variation of curvature, for both branches of the bifurcation. Approximately, one can consider the systolic phase of the cardiac cycle in-health as involving two main events. The first one is characterized by the beginning of ventricular contraction, during which very little of the contents of the ventricles is ejected. However, the cardiac muscle tends to squeeze shut the intramural arteries, thereby markedly increasing outflow resistance for the

blood flow in the epicardial coronary arteries which supply them. This, in turn, attenuates the flowrates in the epicardials, and there is increase in curvature in the epicardials. The second event is characterized by the ventricular contraction, in which most of the ventricular ejection occurs. Since the volume enclosed by the ventricles is reduced, the curvature of the epicardials tends also to be increased further. The ejection fraction (the percentage of the blood volume in a ventricle at the beginning of systole which is ejected by the end of systole) may vary for reasons well-known to physiologists. Therefore, the variation in curvature may vary correspondingly, but the trend is there. For the diastolic phase in the cardiac cycle the ventricles are re-filled, the intramural arteries fill out and, with the corresponding decrease in outflow resistance, the flow in the epicardials increases. Correspondingly, the curvature of the epicardials decreases as the blood volume in the ventricles rises.

In cardiac disease other effects can arise. For example, if there is an infarcted region of myocardium, the cardiac muscle in that region will not contract like healthy muscle, so the epicardial blood flow variation may be changed, as well as the deformations of the ventricular wall masses. If the infarct is due to current thrombotic obstruction, outflow resistance in the corresponding intramural segments is not relieved in diastole. Matsuo et al. [16] have connected change in phasing information to aortic regurgitation. They used a bidirectional Doppler flowmeter catheter to examine coronary flow velocity in patients who had aortic valve disease. The results showed a decreased diastolic and increased systolic coronary flow. In some cases the diastolic flow velocity was less than systolic. These flow velocity patterns became very dominant in severe aortic regurgitation. Such phenomena have a direct effect on the *phase difference* between the arterial motion we study and the pulsatile inflow we impose in our models.

While approximate values for epicardial artery curvature and its variation through a heartbeat are known, precise values are problematic to obtain. Cardiac muscle has a complicated, multi-layered structure with muscle fiber orientation varying in the depth of the ventricular walls. Stevens & Hunter describe a model for pig hearts [17]. Estimation of the phasic variation of coronary artery blood flow, as described recently in [18] involved constraining the form of the velocity profile across the vessel radius, a rather strong assumption that we do not adopt in the present work. Similarly, current modeling of ischemic situations as exemplified in [19] shows that, while progress has been made in representing constituent aspects, there is still much to be done to achieve a functional model.

The alternative route of seeking geometric information from experiment, as in [11], also has its limitations. Biplane or multiplane angiograms taken *in vivo* are useful for estimating axes of vessel segments through the cardiac cycle but do not register luminal diameters or details sufficiently accurately, and do not show artery wall tissue characteristics. Intravascular ultrasound can supply luminal geometry and wall tissue information but does not of itself

find vessel curvature, takes some time to generate *in vivo*, and is limited to larger-diameter coronary vessels. MRI, while potentially providing geometric information and wall structure details for coronary arteries, is still not at a state-of-art where spatial resolution is as good as desired for the current study. Thus, to explore fluid dynamic features of curvature variation as well as curvature and flow pulsatility we have chosen to examine flow in a branched vessel model with prescribed but representative values for the parameters.

2 Basic Assumptions

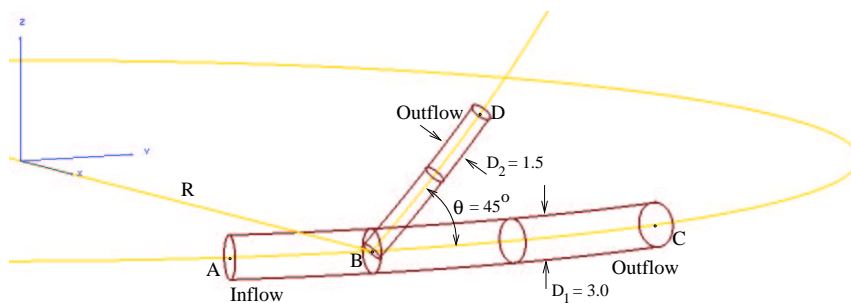


Figure 1: Geometry of the bifurcation and coordinate system. The dimensions are in *mm*.

A three-dimensional geometry model is built as an analytical intersection of two cylindrical tubes which lie on a sphere that represents an idealized heart surface (Figure 1). The heart motion is simulated by changing the sphere radius, R . In [20] the dynamics of coronary artery curvature was obtained from biplane cineangiograms. The results of this study suggest that there is significant harmonic content up to 6 Hz in curvature variation and this was taken into account in the numerical studies in [15, 21]. Here we have adopted the same range of parameters as in [15, 21] and take the frequency of sphere radius variation to be 5Hz, thus the period is $T = 0.2s$. More specifically, R is specified as a sinusoidal function

$$R(t) = R_0(1 + \delta \sin(2\pi t/T)),$$

where the mean sphere radius R_0 is set to 56.25 *mm*. Three different values of parameter δ were used in simulations, 0.0, 0.1 and 0.3. In addition, two cases were considered with $\delta = 0.0$ and R equal to 50.625 and 61.875 *mm*, i.e., minimum and maximum radii for the dynamic case with $\delta = 0.1$.

The tubes have a circular cross section with constant diameters of $D_1 = 3$ *mm* and $D_2 = 1.5$ *mm*. At time $t = 0$ the length of the segments AB , BC and BD are equal to

10.125, 24.0 and 12.375 *mm*, respectively. The lengths of arterial segments are fixed in time so that the total volume of the model remains constant. The junction angle θ is equal to 45° , which is different than the bifurcation modeled in [15]. The origin of the cartesian coordinate system is at the center of the sphere. The axis of the large tube is located in the *xy*-coordinate plane while the small tube is in the $z > 0$ half-space. The point of intersection of the tube axes B lies on the *x*-coordinate axis during the entire cardiac cycle. Thus, the total motion of the model can be separated into a solid body movement and a deformation due to curvature variation. The blood is assumed to be incompressible, Newtonian and homogeneous fluid. The flow is three-dimensional and unsteady, and the Reynolds number defined by $Re = D_1 U_0 / \nu$ is equal to 300, which is a typical value for blood flow in large coronary arteries. Here U_0 is the mean inflow velocity.

3 Methods and Verification

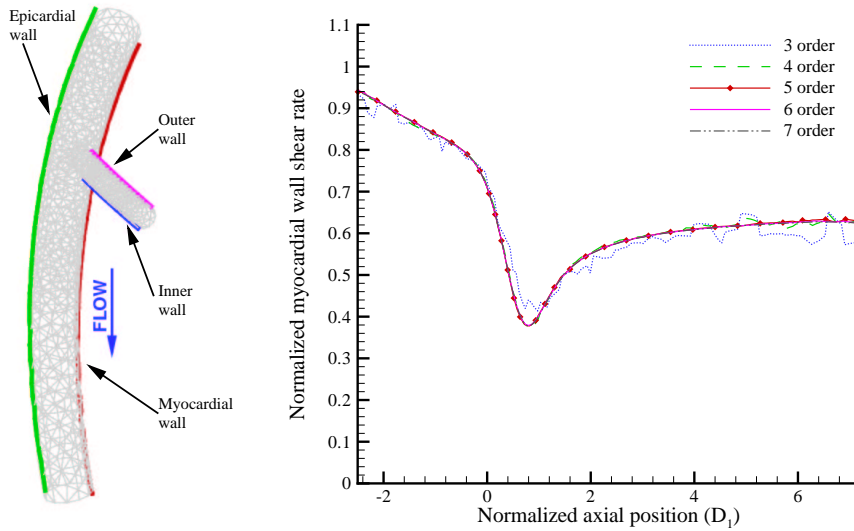


Figure 2: Wall shear rate versus polynomial order (p-refinement). The wall shear rate is extracted along the myocardial wall ($\delta = 0.0$, $\varepsilon = 0.0$). The distance is measured from the intersection point of the tube axes (point B in figure 1) and normalized by the large tube diameter D_1 .

The three-dimensional, unsteady, incompressible Navier-Stokes equations are cast in an arbitrary Lagrangian Eulerian (ALE) frame and solved using the parallel solver NEKTAR that employs the new generation of spectral/ hp element methods [22]. The underlying mesh involves standard finite elements consisted of hexahedra or tetrahedra while convergence is obtained by a dual path: either by h-refinement (increasing the number of elements) or by p-refinement (increasing the polynomial expansion order). This dual resolution distribution allows good load balancing for parallel computation and robustness in the quality of the solution to relatively large mesh deformations.

In the ALE formulation the mesh moves with an arbitrary velocity, therefore the formulation is appropriate for problems with computational domains that are changing in time. There are typically two steps in the development of the mesh for such an ALE simulation: First, the construction of the mesh, and second, its updating during the computation. Both steps are important and can affect the accuracy of the solution [23]. The mesh was constructed using the commercially available mesh generator Gridgen [24], which is appropriate for polymorphic elements. The initial domain corresponds to the model geometry with sphere radius R equal to R_0 . The mesh consists of 6,649 tetrahedral elements. The three-dimensional surface discretization of the domain is shown in Figure 2(left). In the second step, a velocity isotropic smoothing method is used for updating the mesh. In particular, given the velocity W on moving surfaces of the domain this method is applied to find the spatial distribution of W such that element distortion is minimized. More advanced techniques can also be used [23, 25], however this smoothing method produced good results in this study. At each time step, the mesh velocity W is obtained by solving $\nabla^2 W = 0$ with Dirichlet conditions on the boundary of the computational domain. The advantage of the ALE formulation combined with high-order is that the simulation can be run *without remeshing* during computations. Although, as mentioned earlier, the mesh updating method used in this study is not the most efficient, no degradation in the mesh quality was observed.

As was detailed in the introduction, the normal pattern of coronary flow velocities is characterized by a small forward flow during systole and a large forward flow during diastole. A rather complicated coronary flow velocity waveform was measured using doppler flowmeter catheter in [16]. However, due to lack of detailed information here we use a simple time-dependent sinusoidal function to represent this effect. More specifically, at the *inflow* the pulsatile flat velocity profile is specified

$$U(t) = U_0(1 + \varepsilon \sin(2\pi t/T + \frac{\alpha\pi}{180})), \quad U_0 = 400 \text{ mm/s}.$$

Note that here we allow for a phase difference α between the flowrate and the arterial motion; we will investigate systematically this difference for four different values of α in the

δ	0.0	0.1	0.0	0.1	0.1	0.1	0.1	0.1min*	0.1max*	0.3	0.0	0.3	0.3
ε	0.0	0.0	0.1	0.1	0.1	0.1	0.1	0.0	0.0	0.0	0.3	0.3	0.3
$\alpha(deg)$	0	0	0	0	90	180	270	0	0	0	0	0	180

Table 1: Summary of cases simulated.

next section. The parameter ε is set to 0 for simulations with constant inflow velocity. In pulsatile cases, ε is set to 0.1 or 0.3. At the two *outflow* sections (main and side branch) a constant pressure and zero normal derivatives of velocity are imposed; no-slip conditions are used at the vessel walls. To obtain a time-periodic solution the simulations were run for three time periods, $3T$.

To ensure mesh-independence of the computational results, several resolution studies were performed. The mesh was fixed at a position with the sphere radius R equal to R_0 . The resolution was then increased by increasing the polynomial expansion order in each element, i.e. by p-refinement. Due to the sharp edge at the junction of arterial segments there is a numerical singularity in solution. It is localized in small region close to junction and does not seem to affect the results in other parts of domain. A typical plot of the convergence rate by p-refinement is shown in Figure 2(right). Here, the values of wall shear rate, extracted along the curve on the myocardial wall, are plotted against the distance from the intersection point of tube axes of the model, normalized by the large tube diameter (D_1). In all simulations described below fifth-order ($p = 5$) polynomial expansion was used uniformly for all elements. The time step independence of the results was verified for the case with dynamic curvature variation ($\delta = 0.1$) and pulsatile inflow ($\varepsilon = 0.1$). The time step was divided by two and computational results were compared against the results with the original timestep; no differences were found.

4 Results

A summary of the cases we have simulated is shown in table 1. In two cases marked with * the geometry was fixed at the minimum and maximum radii for the dynamic case with $\delta = 0.1$, which correspond to R equal to 50.625 mm and 61.875 mm , respectively.

In the following we present results for representative cases only.

Velocity field and secondary flow structure

In most simulations the main features of the flow are quite similar to the results with steady inflow and static geometry ($\delta = 0.0$ and $\varepsilon = 0.0$). The core of the flow in the main branch is shifted towards the epicardial wall. The secondary flow structure in selected cross-sections of the main branch is shown in Figure 3. There is a Dean type vortex structure in the main branch, which is typically seen in flows in curved tubes. The fluid moves from the myocardial wall to the epicardial wall along the diameter, and then returns to the myocardial wall along the sides of the tube, forming two counter-rotating vortices. The vortical structures are symmetric before one large tube diameter D_1 from the point of intersection of tube axes. The presence of a side branch results in the skewing of vortices and loss of symmetry, which can be seen up to three large tube diameters beyond the bifurcation. The shift of the flow core towards the epicardial wall in the main branch results in an overall rotating fluid motion in the side branch beyond the bifurcation, which shortly disappears due to viscous forces (not shown here). The secondary flow is weak in the side branch (about four small tube diameters from the bifurcation), and counter-rotating vortices are hardly seen.

The dynamic geometry and pulsatile inflow can significantly change the secondary flow structure. In Figure 4 we show the effect of the motion and variation of curvature during each cardiac cycle on the secondary flow structure for the simulation case with parameters $\delta = 0.3$ and $\varepsilon = 0.0$. The secondary flow structure in the main branch is shown at a fixed cross-section beyond the bifurcation at different time moments during the simulation cycle. We see that there is a significant qualitative change in the flow patterns for the four phases shown in the figure, which are different from the stationary case.

Flowrate through the branches

The dynamic geometry and pulsatile inflow affect the flow distribution between the two branches of the model. Figure 5 shows the variation of the flowrate ratio between the main and the side branch during the periodic cycle for different simulations. In all simulations there is a *phase difference* between variation of curvature or inflow velocity and flowrate ratio variation. In the simulation with fixed averaged geometry and steady inflow the flowrate ratio between the side and the main branch is 0.123. Both dynamic geometry and pulsatility can result in more than 20% change in the value of the flowrate ratio. In the simulation with dynamic geometry and steady inflow ($\delta = 0.1$, $\varepsilon = 0.0$), the variation is clearly due to the motion of the artery as it lies on the surface of the simulated heart. The difference in flowrate through the side branch is found to be insignificant in quasi-static simulations, when the geometry is fixed with mean, minimum and maximum curvature radii. The combined

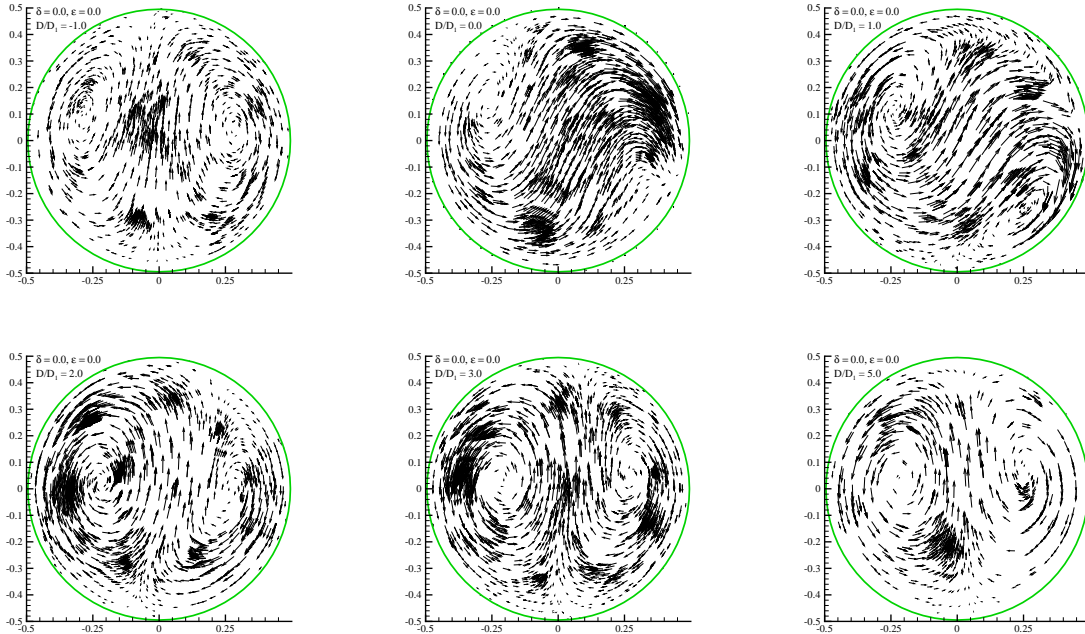


Figure 3: Secondary flow structure for the reference case ($\delta = 0.0$, $\varepsilon = 0.0$). The flow is out of the page and the bifurcation point is at $D/D_1 = 0.0$.

effect of dynamic geometry and pulsatile inflow depends strongly on the phase difference angle α . In the simulation with $\alpha = 90^\circ$ the variation is the least of all simulated cases (less than 5%). The maximum variation is observed for $\alpha = 270^\circ$ and is equal to 51%.

Wall Shear Rate

Next we examine the distribution of the wall shear rate (WSR) at selected cross-sections of the main and side branch. The cross-sections are taken perpendicular to the tube axes at certain distances from the intersection point of axes of main and side branches. The distance is normalized by the large or small tube diameter for the main or side branch cross-sections, respectively. The extracted values of the WSR are normalized by the magnitude of the wall shear rate in a straight pipe with the same diameter, flowrate and Reynolds number. The same normalization of WSR is used for all results presented in this section. For the simulation with steady inflow and fixed (in the mean) position geometry ($\delta = 0.0$, $\varepsilon = 0.0$)

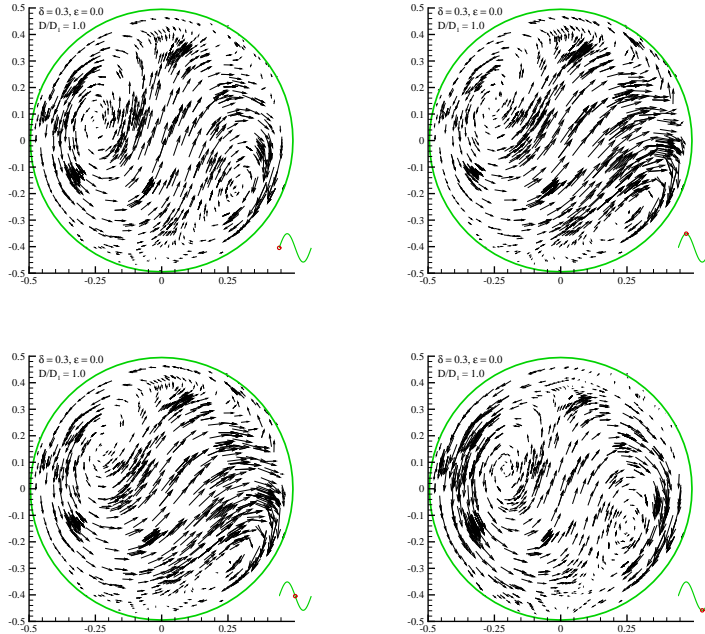


Figure 4: Secondary flow structure for the case ($\delta = 0.3, \varepsilon = 0.0$) The flow is out of the page ($D/D_1 = 1.0$).

the highest values of the WSR are observed on the side branch wall of the main branch beyond the bifurcation. In general, WSR is lower on the myocardial wall of the main branch than on epicardial wall, which can be related to the curved geometry of the model. Low values of WSR are also observed on the outer wall of the side branch close to bifurcation. The effect of curvature on the WSR distribution is not pronounced in the side branch. In general, the time-averaged WSR of all the simulations we studied give results similar to the steady inflow and fixed geometry case (see Figure 6). This is consistent with previous findings in [11, 15] but somewhat surprising due to the large temporal variation especially for certain values of the phase difference, as we shall see next.

The effect of dynamic geometry ($\delta = 0.1, \varepsilon = 0.0$) on the wall shear rate is shown in Figure 7. The variations of WSR along the myocardial wall of the main branch are significant in comparison to its low mean. The region of the largest variation of WSR during the cycle is located on the surface of the side branch. This can be attributed to the significant variation of the flowrate through the branch.

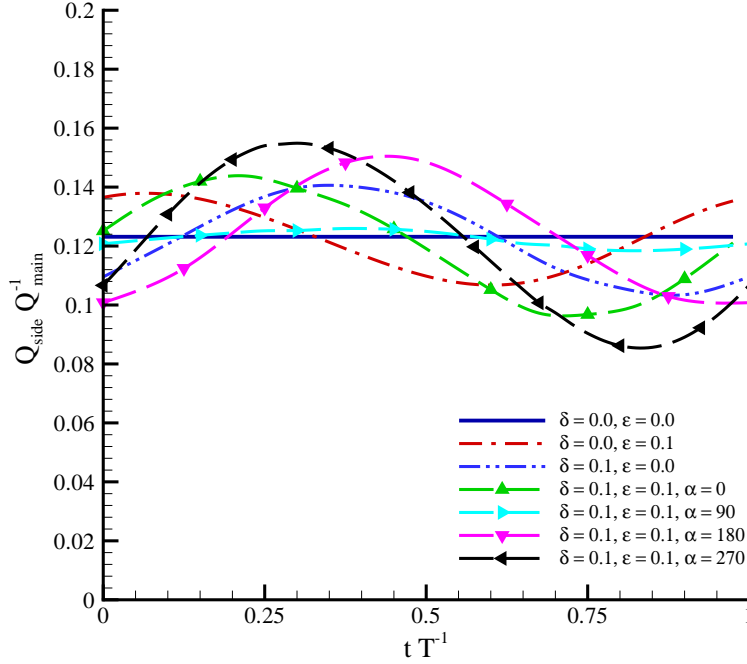


Figure 5: Flowrate ratio time-variation for different simulation cases.

The effect of pulsatile inflow on WSR ($\delta = 0.0$, $\varepsilon = 0.1$) is shown in Figure 8. The variation of WSR during the cycle is large, in comparison to the simulation with dynamic geometry and steady inflow. This is in agreement with the results reported in [11] for a single coronary artery without a side branch. In our case, this can be related to the variation of the total mass flow through the model.

Results related to the combined effect of pulsatility, unsteady geometry, and phase difference on mean (i.e., time-averaged) values and variation of WSR during the periodic cycle are shown in Figures 9 to 12. Results are shown for the simulation cases with parameters $\delta = 0.1$, $\varepsilon = 0.1$ and phase difference α equal to 0, 90, 180 and 270 degrees. The dependence of the variation of WSR in the main branch on the phase difference is found to be less pronounced before the bifurcation than after. For the simulation cases with $\alpha = 90^\circ$ and $\alpha = 180^\circ$ the variation of WSR before the bifurcation in the main branch is larger on the myocardial wall than on epicardial. The opposite is observed in simulations with $\alpha = 0^\circ$

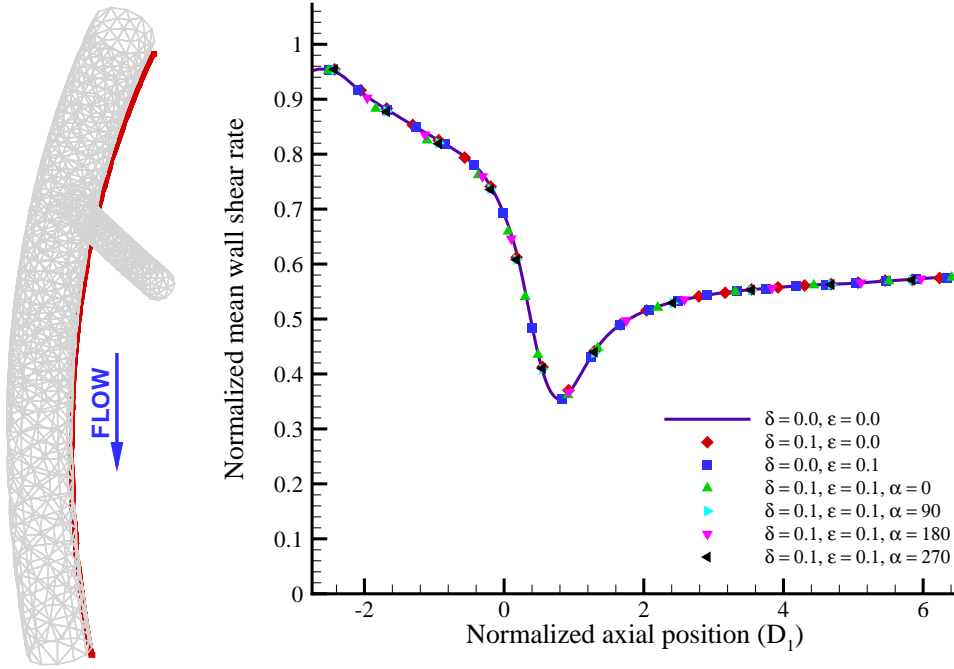


Figure 6: Normalized *time-averaged* wall shear rate extracted along the myocardial wall for different simulation cases.

and $\alpha = 270^\circ$. One large tube diameter beyond the bifurcation in the main branch, both minimal and maximal variations of WSR are observed in simulation with phase difference equal to 270 degrees. More specifically, the minimum is located on the myocardial wall, while the maximum on the side branch wall. At the same time, maximal variation of the WSR on the myocardial wall and minimal variation on the side branch wall are observed in simulation with $\alpha = 90^\circ$. The magnitude of the time-dependent WSR on the myocardial wall becomes very low during the periodic cycle in this simulation. Further beyond the bifurcation the dependence of the WSR variation on the phase difference becomes less pronounced. In the side branch the overall variation of the WSR depends strongly on α . Minimal variation is observed when $\alpha = 90^\circ$ while maximal variation is observed when $\alpha = 270^\circ$. In the latter case, the minimum of the magnitude of the WSR on the outer wall of the side branch during the periodic cycle is very low.

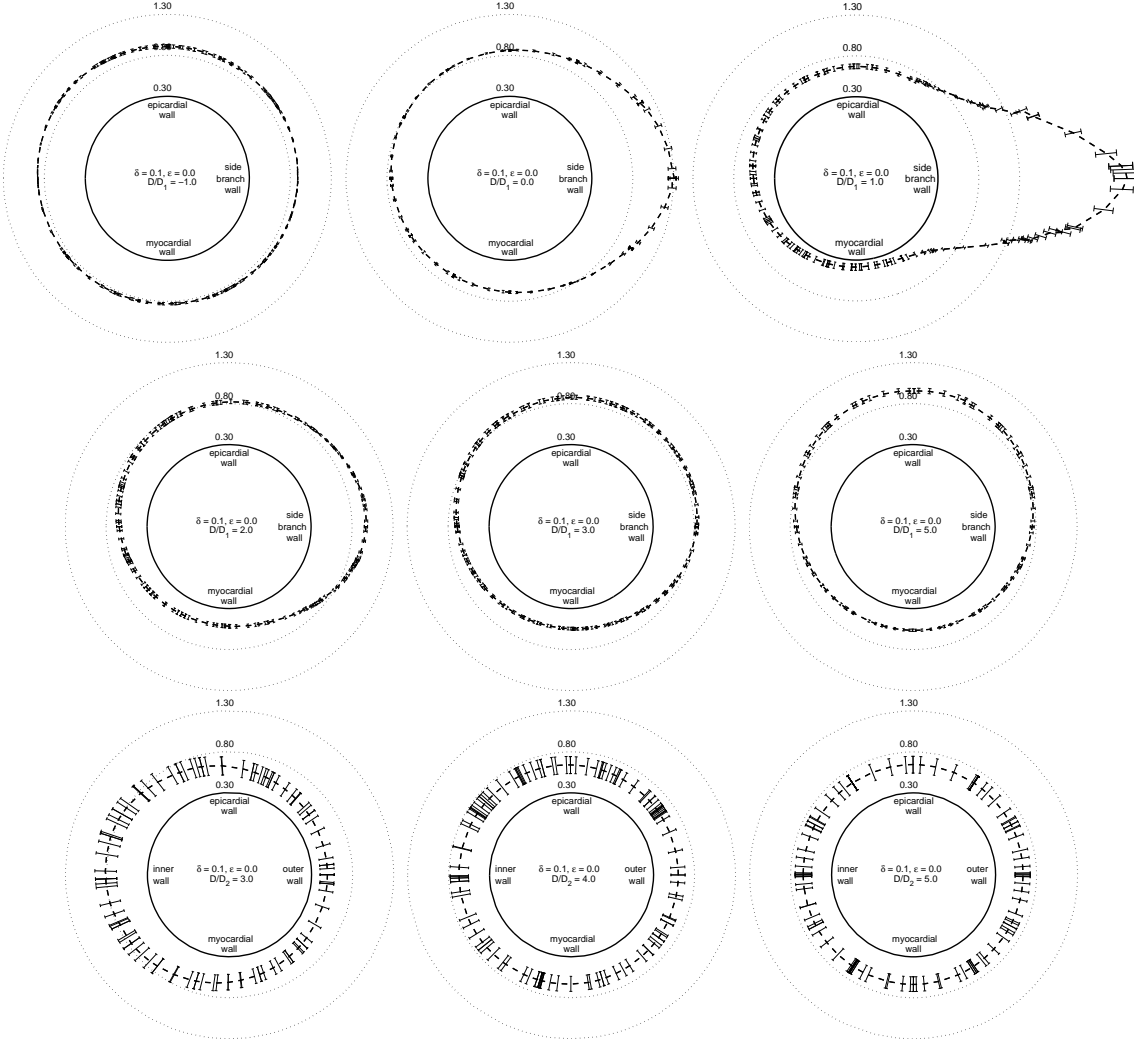


Figure 7: Wall shear rate, mean (time-averaged), and variation during the periodic cycle. The cross-sections are taken perpendicular to the tube axes at certain distances from the intersection point of axes of main and side branches. The distance is normalized by the large or small tube diameter for the main or side branch cross-sections, respectively. The extracted values of the WSR are normalized by the magnitude of the wall shear rate in a straight pipe with the same diameter, flowrate, and Reynolds number. The results shown are for the case with dynamic geometry and steady inflow ($\delta = 0.1$, $\epsilon = 0.0$).

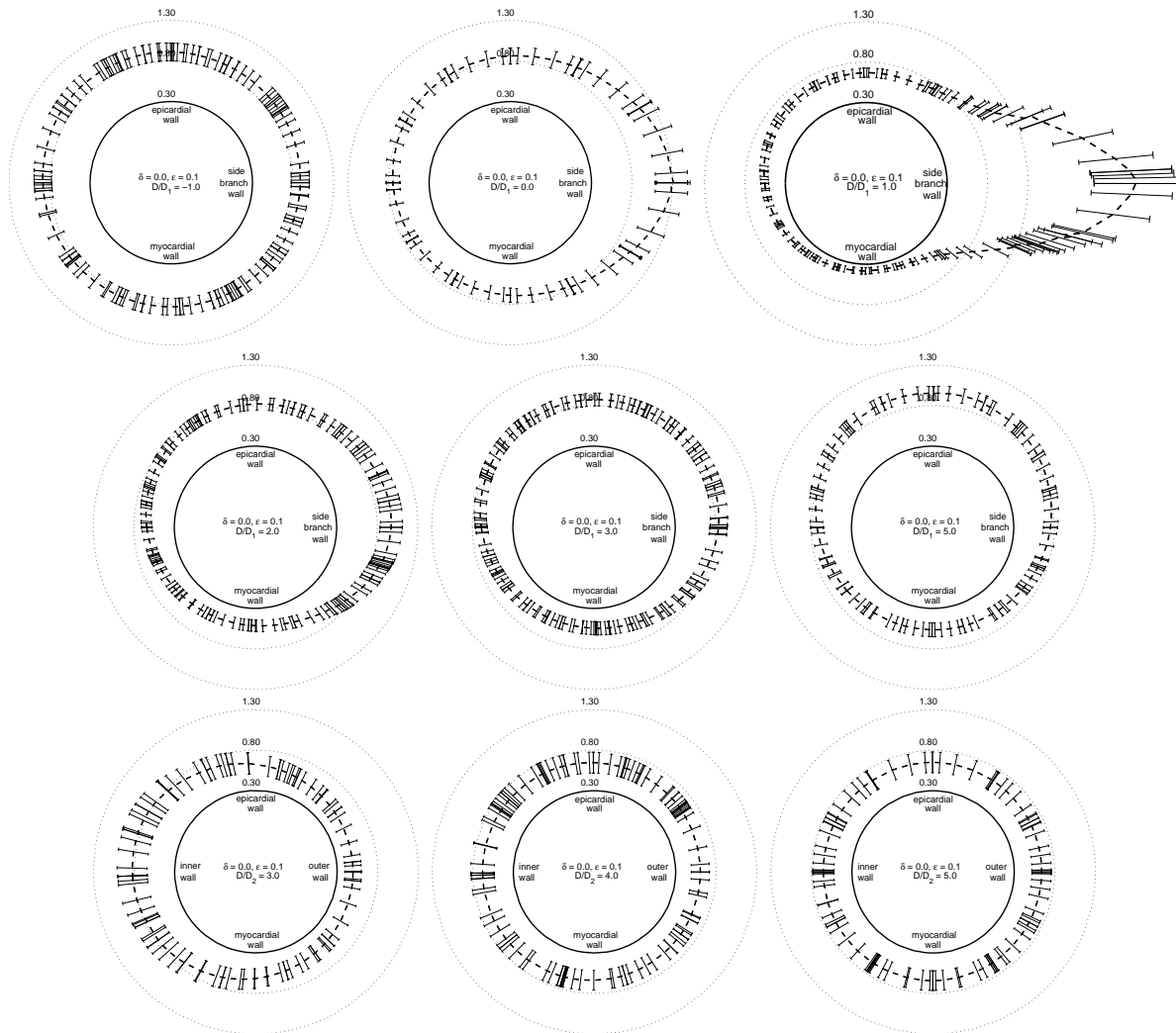


Figure 8: The effect of pulsatile inflow on WSR ($\delta = 0.0$, $\varepsilon = 0.1$). Same legend as in Figure 7.

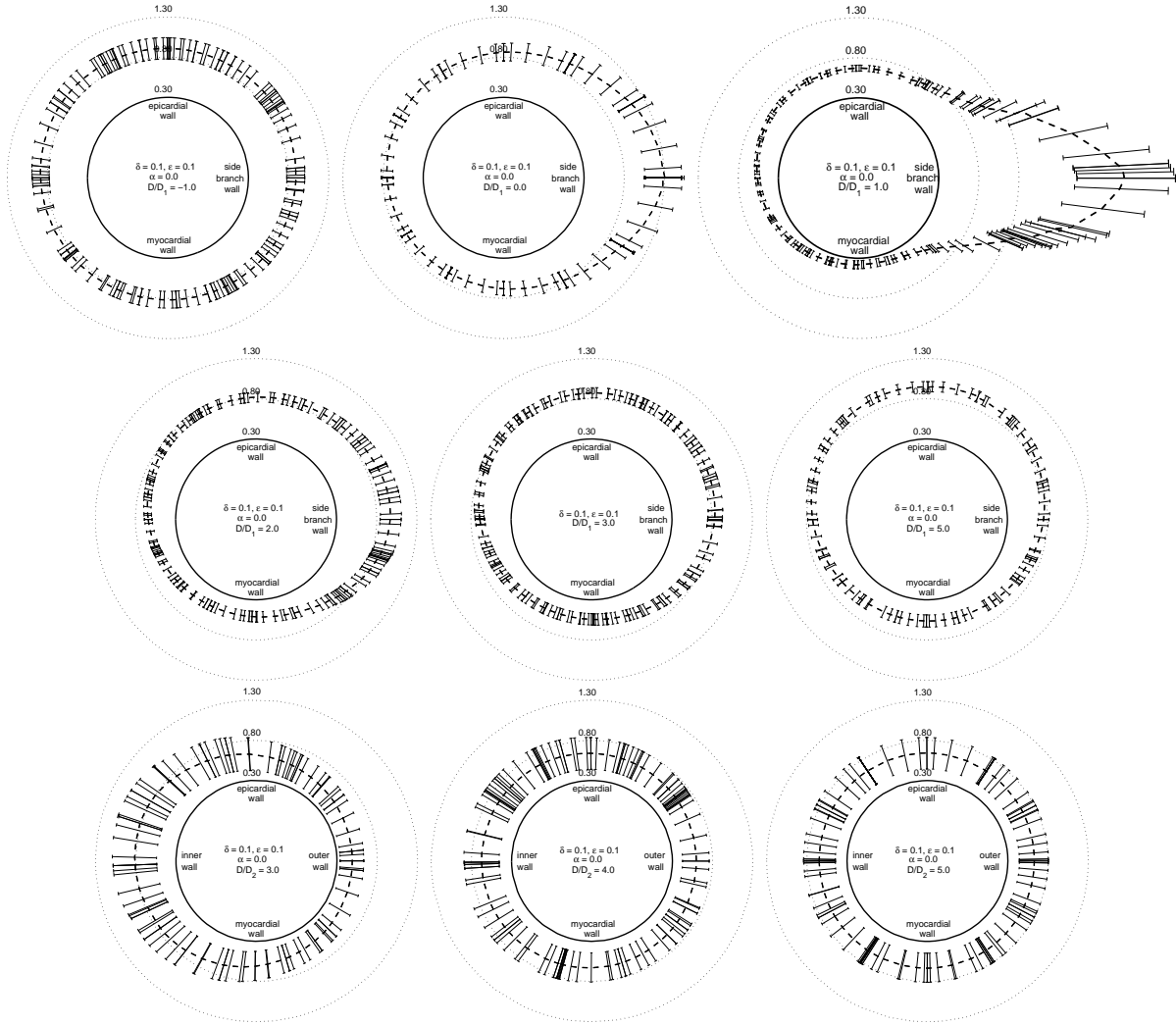


Figure 9: The combined effect of dynamic geometry, pulsatile inflow and phase difference angle on the mean values and variation of WSR during the periodic cycle. Simulation parameters: $\delta = 0.1$, $\varepsilon = 0.1$, $\alpha = 0$.

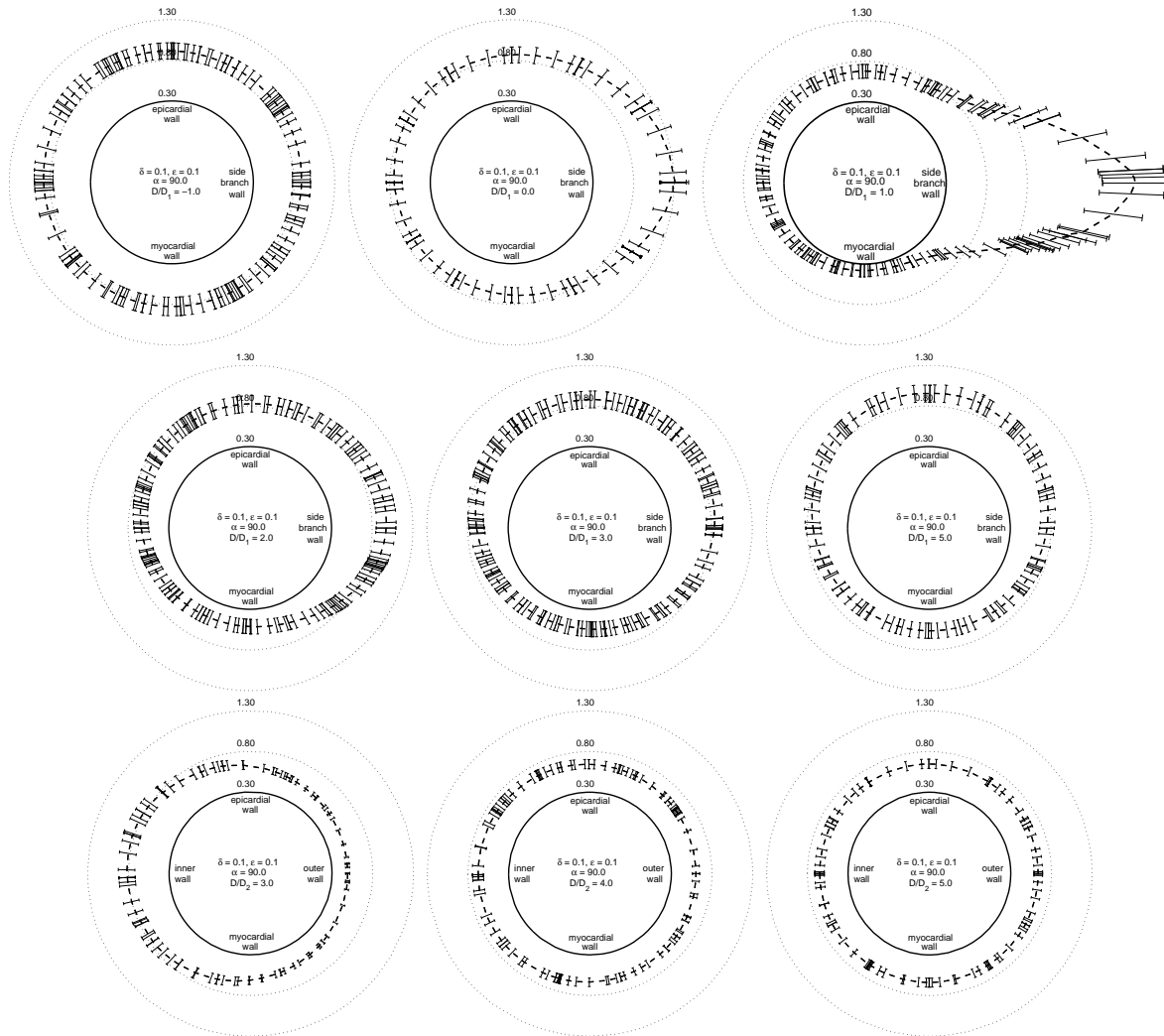


Figure 10: Same legend as in Figure 9. Simulation parameters: $\delta = 0.1$, $\varepsilon = 0.1$, $\alpha = 90$.

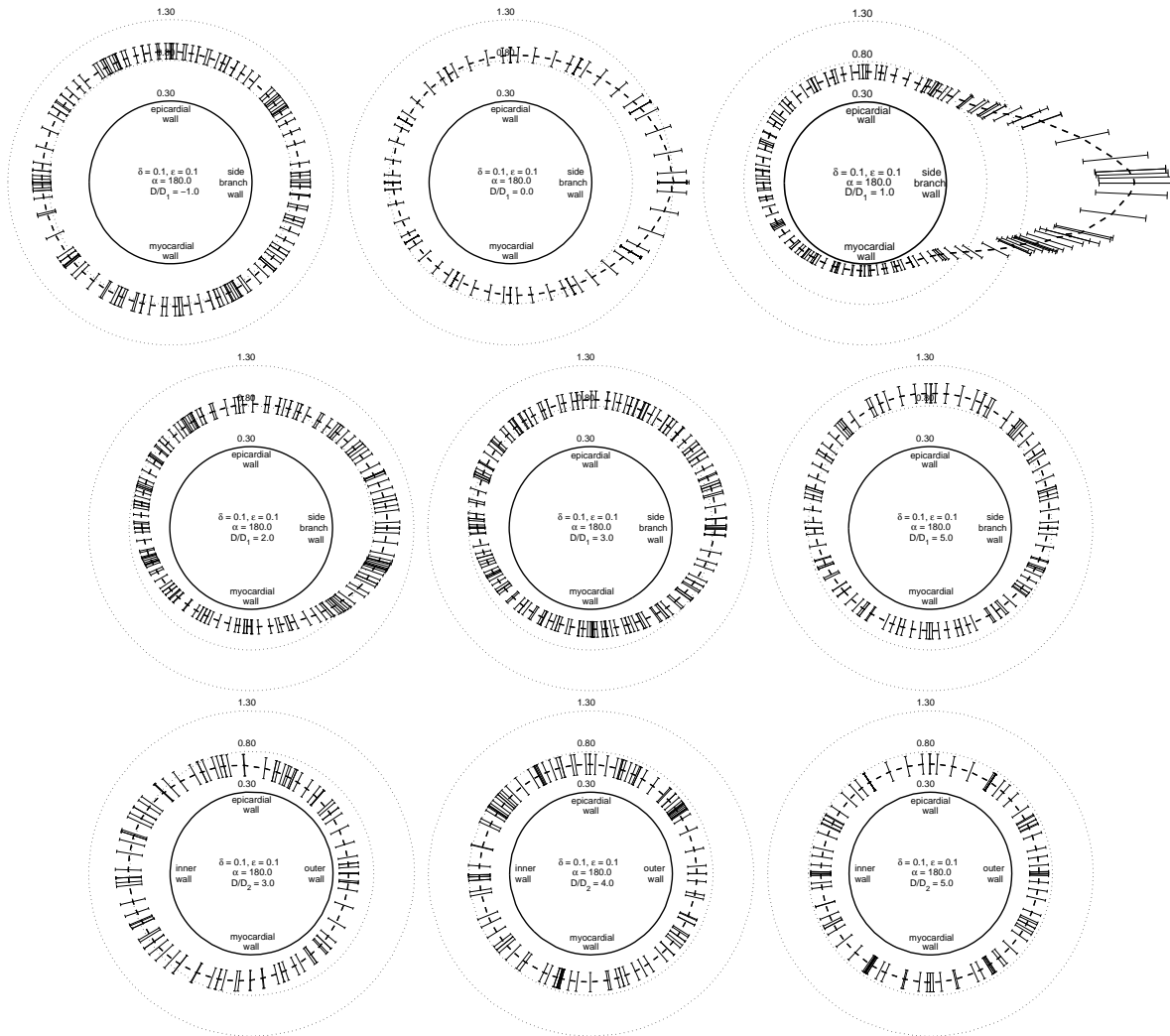


Figure 11: Same legend as in Figure 9. Simulation parameters: $\delta = 0.1$, $\epsilon = 0.1$, $\alpha = 180$.

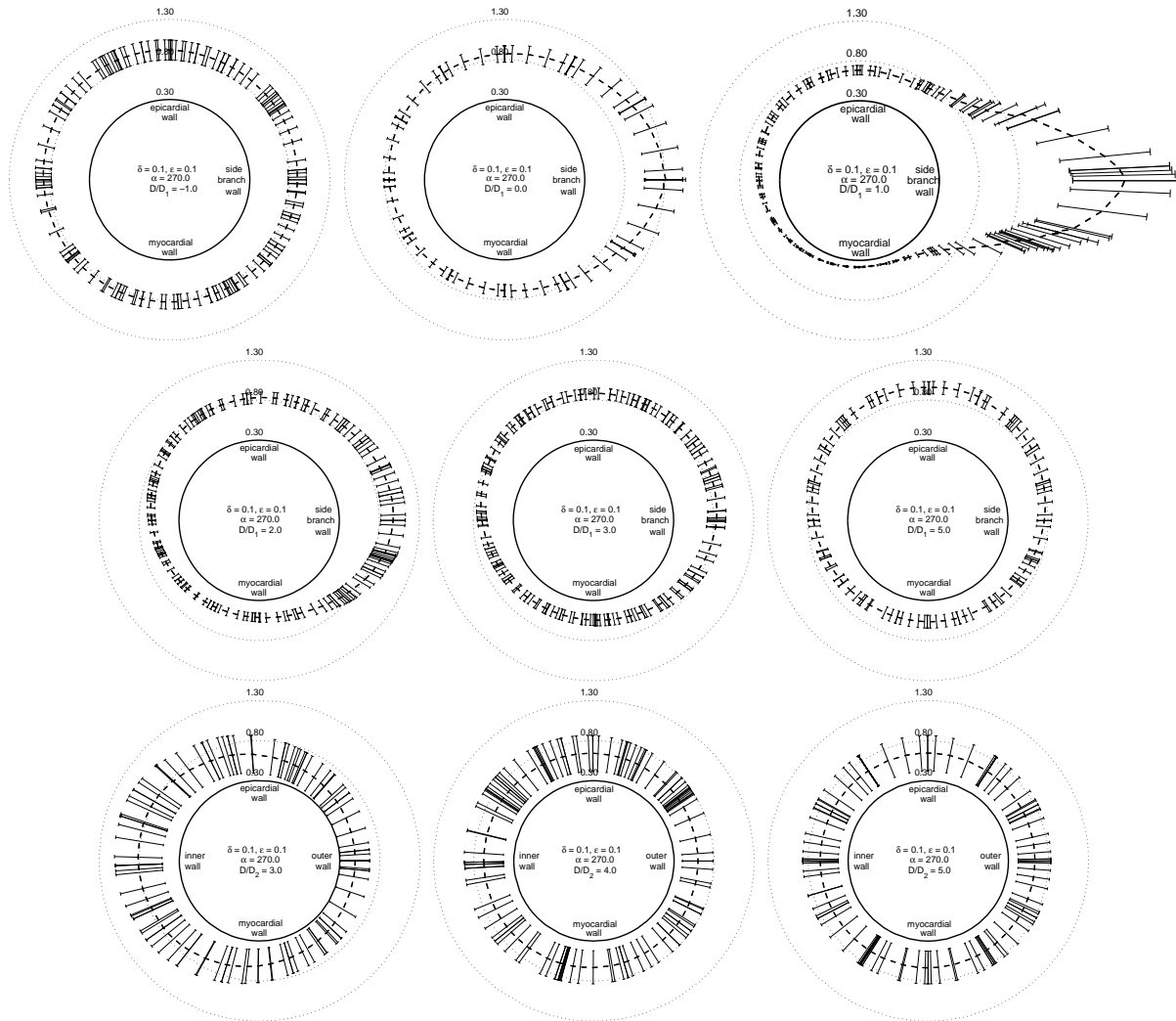


Figure 12: Same legend as in Figure 9. Simulation parameters: $\delta = 0.1$, $\varepsilon = 0.1$, $\alpha = 270$.

Effect of the variation amplitude on NWSRA

To characterize the variation of WSR during the cycle we use the normalized wall shear rate amplitude (NWSRA). This quantity was introduced in [12] and also used in [15] as this quantity may be more relevant to atherogenesis research compared to the dimensional WSR amplitudes, which are of more interest from a fluid dynamics perspective. It is defined as the difference between the maximum and minimum values of the WSR during the cycle, divided by the mean ($\delta = 0.0, \varepsilon = 0.0$) WSR.

In general, in all simulations the increase of parameters δ and ε results in increase of the variation of flowrate ratio between branches and wall shear rate. Figure 13(a) shows the NWSRA for the simulation with dynamic geometry and steady inflow ($\delta = 0.1, \varepsilon = 0.0$). The values are extracted along selected lines on the myocardial and epicardial walls of the main branch, and the inner and outer walls of the side branch. The distance is measured from the intersection point of the tube axes and normalized by the large tube diameter D_1 . In Figure 13(b) we can see similar results for the simulation with the amplitude of curvature variation three times larger ($\delta = 0.3, \varepsilon = 0.0$). The values of NWSRA are proportionally larger compared to the case with $\delta = 0.1$.

Combined effect of δ , ε and α on NWSRA

Figure 14 demonstrates the combined effect of curvature, inflow velocity and phase difference variations on NWSRA. The values of the NWSRA are extracted along the myocardial wall of the main branch. The distance is measured from the intersection point of tube axes and normalized by large tube diameter.

We can subdivide the figure into three vertical regions. The first region corresponds to the part of myocardial wall, located before the intersection point of axes, which is marked with 0 (zero on the horizontal axis) in the figure. The second region extends from this point up to three large tube diameters. The third region includes the rest of the figure. In the first and third regions the main contribution to the NWSRA is from the pulsatility of the flow. The extracted values for non-pulsatile simulation are significantly lower. The dependence of the NWSRA on the phase difference α is found to be strong and can change the results even qualitatively as shown in the figure for region two. In general, in the second region, the dependence of the NWSRA on the simulation parameters is less intuitive. In two simulation cases, ($\delta = 0.0, \varepsilon = 0.1, \alpha = 0^\circ$) and ($\delta = 0.1, \varepsilon = 0.1, \alpha = 270^\circ$), the distribution of NWSRA differs significantly from other cases. More specifically, there is a local minimum approximately 0.9 large tube diameters below the point of tube axes intersection, while in other simulations a local maximum is observed.

5 Summary and Discussion

In the current paper, we have presented new results for the effect of unsteady geometry on the hemodynamics of the right coronary artery with a bifurcation; these results complement the recently published results in [11]. In that study a realistic arterial motion was considered but no side branches were included in the model. Our results also complement the results reported in [15], where a bifurcation was included in the model but the inflow was steady. In the current study we used a simplified arterial motion and investigated the effects of the combined unsteady motion and flow pulsatility, with focus on the region around the bifurcation. We found that the flowrate ratio between the side branch and the main branch is influenced significantly by the combined unsteady phenomena, and more importantly from the phase difference between them. In one case we computed more than 50% temporal variation in the flowrate ratio!

The time-averaged levels of wall shear rate (WSR) are not affected by the unsteady motion, in accord with the findings in [11, 15]. However, the normalized wall shear rate amplitude (NWSRA), which measures temporal variations, is affected dramatically by the presence of the bifurcation. In particular, the effect of unsteady geometry is to produce a maximum of NWSRA on the myocardial wall close to bifurcation in contrast with a minimum that is produced due to pulsatile inflow. This *qualitative change* in the distribution of WSR depends strongly on the phase difference between the two unsteady phenomena, if the combined effect of dynamic geometry and pulsatile flow is considered. We found, for example, that for the phase difference $\alpha = 0^\circ; 270^\circ$ the WSR temporal variation in the main branch (close to the side branch) is large while the variation of WSR on the myocardial wall is small. On the other hand, the opposite is true for the cases with $\alpha = 90^\circ; 180^\circ$. These results demonstrate the importance of phase difference, an issue that has not been modeled before in computational studies. In experimental work, however, Matsuo *et al.* [16] have addressed this issue for patients with aortic regurgitation. In particular, they found that in patients with dominant aortic regurgitation, the low-diastolic perfusion pressure leaves the epicardial vessels partially collapsed. Thus, with the large increase in pulse pressure during systole, the epicardial vessels can accommodate more blood before the effects of mural and extramural pressure become restrictive. In our model, this will change the minimum and maximum of flowrate with respect to minimum and maximum of the dynamic curvature. This was parameterized with the phase difference α in the current model. Matsuo *et al.* found that α can vary from 0° to 180° in the 14 patients with aortic regurgitation they examined.

So in general, in computational studies there arises an issue of representing the flow wave form accurately. This involves three factors: First, the flow rate rising in early systole -

typically the pressure rise early in systole is fairly rapid, so the phase of that rise is fairly constant, barring some cardiac pathologies. Second, the time-dependence and magnitude of coronary flow rate, the latter being highly dependent on pharmacological intervention. Third, the point in the cardiac cycle at which the zero-flow pressure intercept is reached (or closely approached), and the flow becomes zero (or very small).

In our model, rather than keeping the start of opening of the coronary artery flow linked to a fixed point in the cycle, and varying the relative time-span of flow above zero, we have kept the waveform of the coronary flow uniform among our cases described here and varied the phase at which it started, relative to curvature of the flexing vessel. One of the reasons to investigate this is that there can be some cardiac pathologies, which might lead to corresponding circumstances, and shifts in mural transport which might accompany them might then be reflected in different geometric development of lesions.

Clearly, the limitations of the current study are the idealized geometry and idealized arterial motion. Better models can be introduced for the arterial motion by replacing the sphere with an ellipse and allowing torsional motion as well. Also, realistic or more accurate models for the flowrate waveform can be readily adopted. However, this introduces many more parameters in the system that may not be required, from the fundamental understanding standpoint, at this initial stage of modeling these complex phenomena. Comparing with previous findings in the works reported in [11, 12, 13], which considered both realistic and idealized motions but for a single artery, we see that such differences have only produced quantitative differences. The presence of the bifurcation as well as accounting for nonzero values of phase difference, however, seems to indicate that there are qualitative differences, as our present findings have shown.

Acknowledgement

This work was supported by an NSF-ITR grant (CCR-0086065) and by BSF (IBSF 2001150). We would like to thank S.J. Sherwin of Imperial College and Z. Yosibash and A. Yakhot of Ben Gurion University for useful discussions. Computations were performed on the AHPCC Los Lobos Linux cluster.

References

- [1] M. Ojha, R.L. Leask, J. Butany, and K.W. Johnston. Distribution of intimal and medial thickening in the human right coronary artery: A study of 17 RCAs. *Atherosclerosis*,

158:147, 2001.

- [2] T. Karino, T. Asakura, and S. Mabuchi. Flow patterns and preferred sites of atherosclerosis in human coronary and cerebral arteries. In Y. Yoshida, T. Yamaguchi, C.G. Caro, S. Glagov, and R.M.Nerem, editors, *Role of Blood Flow in Atherogenesis*, page 67. Springer-Verlag, 1988.
- [3] C. Velican and D. Velican. The precursors of coronary atherosclerotic plaques in subjects up to 40 years old. *Atherosclerosis*, 37:33, 1980.
- [4] D.N. Ku, C.K. Zarins, D.P. Giddens, and S. Glagov. Early atherosclerosis and pulsatile flow in the human carotid bifurcation. In Y. Yoshida, T. Yamaguchi, C.G. Caro, S. Glagov, and R.M.Nerem, editors, *Role of Blood Flow in Atherogenesis*, page 73. Springer-Verlag, 1988.
- [5] D.A. Steinman, T.L. Poepping, M. Tambasco, R.N. Rankin, and D.W. Holdsworth. Flow patterns at the stenosed carotid bifurcation: Effects of concentric versus eccentric stenosis. *Annals of Biomedical Engineering*, 28:415, 2000.
- [6] C. Bertolotti and V. Deplano. Three-dimensional numerical simulations of flow through a stenosed coronary bypass. *Journal of Biomechanics*, 33:1011, 2000.
- [7] D.A. Steinman, J.B. Thomas, H.M. Ladak, J.S. Milner, B.K. Rutt, and J.D. Spence. Reconstruction of carotid bifurcation hemodynamics and wall thickness using computational fluid dynamics and MRI. *Magnetic Resonance in Medicine*, 47:149, 2002.
- [8] J.G. Myers, J.A. Moore, M. Ojha, K.W. Johnston, and C.R. Ethier. Factors influencing blood flow patterns in the human right coronary artery. *Annals of Biomedical Engineering*, 29:109, 2001.
- [9] S.Z. Zhao, X.Y. Xu, A.D. Hughes, S.A. Thom, A.V. Stanton, B. Ariff, and Q. Long. Blood flow and vessel mechanics in a physiologically realistic model of a human carotid arterial bifurcation. *Journal of Biomechanics*, 33:975, 2000.
- [10] K. Perktold and G. Rappitsch. Computer simulations of local blood flow and vessel mechanics in a compliant carotid artery bifurcation model. *Journal of Biomechanics*, 28:845, 1995.
- [11] D. Zeng, Z. Ding, M.H. Friedman, and C.R. Ethier. Effects of cardiac motion on right coronary artery hemodynamics. *Annals of Biomedical Engineering*, 31:420, 2003.

- [12] A. Santamarina, E. Weydahl, J.M. Siegel, and J.E. Moore. Computational analysis of flow in a curved tube model of the coronary arteries: effects of time-varying curvature. *Annals of Biomedical Engineering*, 26:944, 1998.
- [13] S. Schilt, J.E. Moore, A. Delfino, and J.J. Meister. The effects of time-varying curvature on velocity profiles in a model of the coronary arteries. *Journal of Biomechanics*, 29:469, 1996.
- [14] J.J. Smith and J.P. Kampine. *Circulatory Physiology - the Essentials*. Williams and Wilkins, 1990.
- [15] E.S. Weydahl and J.E. Moore. Dynamic curvature strongly affects wall shear rates in a coronary artery bifurcation model. *Journal of Biomechanics*, 34:1189, 2001.
- [16] S. Matsuo, M. Tsuruta, M. Hayano, Y. Imamura, Y. Eguchi, T. Tokushima, and S. Tsuji. Phasic coronary artery flow velocity determined by Doppler flowmeter catheter in aortic stenosis and aortic regurgitation. *American Journal of Cardiology*, 62:917, 1988.
- [17] C. Stevens and P.J. Hunter. Sarcomere length changes in a 3D mathematical model of the pig ventricles. *Progress in Biophysics and Molecular Biology*, 82:229, 2003.
- [18] N.P. Smith, A.J. Pullan, and P.J. Hunter. An anatomically based model of transient coronary blood flow in the heart. *SIAM J. Appl. Math.*, 62:990, 2002.
- [19] P.J. Mulquiney, N.P. Smith, K. Clarke, and P.J. Hunter. Mathematical modeling of the ischemic heart. *Nonlinear Analysis*, 47:235, 2001.
- [20] M.F. Gross and M.H. Friedman. Dynamics of coronary artery curvature obtained from biplane cineangiograms. *Journal of Biomechanics*, 31:497, 1998.
- [21] J.E. Moore, E.S. Weydahl, and A. Santamarina. Frequency dependence of dynamic curvature effects on flow through coronary arteries. *Journal of Biomechanical Engineering*, 123:129, 2001.
- [22] G.E. Karniadakis and S.J. Sherwin. *Spectral/hp Element Methods for CFM*. Oxford University Press, 1999.
- [23] I. Lomtev, R.M. Kirby, and G.E. Karniadakis. A discontinuous Galerkin ALE method for compressible viscous flows in moving domains. *Journal of Computational Physics*, 155:128, 1999.

[24] <http://www.pointwise.com>.

[25] R. Lohner and C. Yang. Improved ale mesh velocities for moving bodies. *Communications in Numerical Methods in Engineering*, 12:599, 1996.

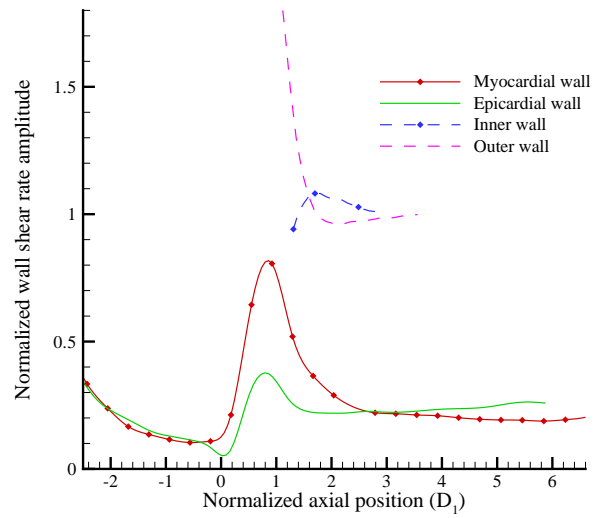
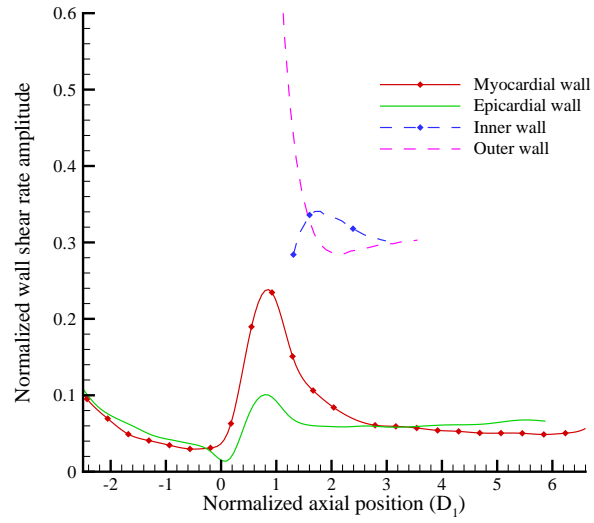


Figure 13: Normalized wall shear rate amplitude. (a) ($\delta = 0.1, \varepsilon = 0.0$); (b) ($\delta = 0.3, \varepsilon = 0.0$).

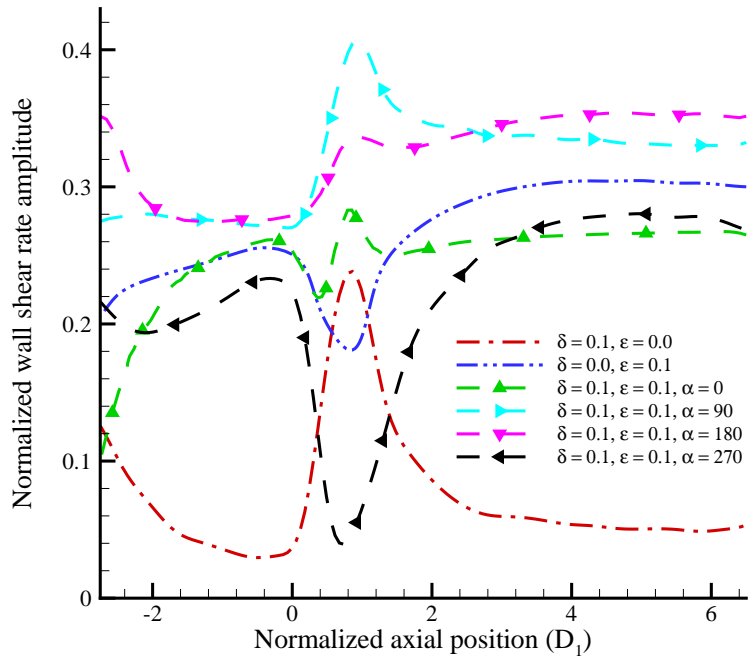


Figure 14: Normalized wall shear rate amplitude extracted along the myocardial wall for different simulation cases.